Theoretical and Applied Fracture Mechanics 127 (2023) 104034

Contents lists available at ScienceDirect

Theoretical and Applied Fracture Mechanics

journal homepage: www.elsevier.com/locate/tafmec

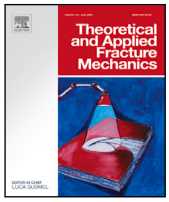

Analysis of crack closure and wake of plasticity with the distributed dislocation technique

James Vidler [a], Andrei Kotousov [a,*], Ching-Tai Ng [b]

[a] The University of Adelaide, School of Electrical and Mechanical Engineering, Adelaide, Australia
[b] The University of Adelaide, School of Architecture and Civil Engineering, Adelaide, Australia

ARTICLE INFO

Keywords:
Crack closure
Strip-yield model
Crack tip plasticity
Fatigue crack growth
Distributed dislocation technique
Chebyshev–Gauss quadrature

ABSTRACT

A new method for the analysis of plasticity-induced closure of finite cracks is developed based on the distributed dislocation technique. The method is applied to analyse closure and opening processes for an embedded fatigue crack propagating under constant amplitude cyclic loading. The obtained solution and presented results can serve as a benchmark for numerical procedures utilising the same yield-strip methodology. Comparison with past numerical studies reveals similar trends, though there are some differences in the crack tip opening values, particularly for low and negative R-ratios. The latter may indicate the need for a better approach to the discretisation of the contact, direct and reverse plasticity zones in the numerical procedures which utilise the same methodology. The developed method is general, and it can be adapted to evaluate the crack tip opening stress for other crack geometries and loading conditions.

1. Introduction

The discovery of the crack closure phenomenon by Elber in 1970 [1] has had a significant impact on the understanding of fatigue phenomena and fatigue crack growth evaluation techniques. Crack closure implies that a fatigue crack remains closed for some portion of a tensile load cycle. The crack closure phenomenon leads to a reduction of the crack driving force, which is often considered to be a function of the effective stress intensity factor range. Crack closure may occur due to several mechanisms, though the present work focuses on plasticity-induced crack closure, where closure occurs due to the formation of a wake of plasticity behind the crack tip. Currently, almost all advanced fatigue life evaluation procedures employ the crack closure concept [2–5].

Though possible in principle, direct application of the 3D Finite Element method to evaluate the crack tip opening loads is extremely challenging, due to the complex nature of the problem, which requires implementation of a crack advance scheme and 3D simulation of contact between the crack surfaces in the presence of large plastic deformations [6–8]. Additionally, it is computationally unfeasible to conduct direct simulations for a very large number of fatigue cycles (hundreds of thousands), which is typical in the high-cycle fatigue regime. Therefore, the analysis is normally undertaken based on the strip-yield model or Dugdale model [9,10]. This idealised model assumes that all plastic deformation is confined to a strip ahead of the crack tip; this assumption greatly simplifies the elastic–plastic analysis, yet still captures essential features, making the underlying framework feasible for use in fatigue life evaluation procedures.

Analytical modelling of crack closure and opening mechanisms using the plane strip-yield model was initiated by Budiansky and Hutchinson [11], who evaluated the crack tip opening stress and other associated parameters (lengths of the contact and reverse plasticity zones, etc.) for non-propagating and propagating semi-infinite cracks at different cyclic stress ratios (R-ratios) using the distributed dislocation technique (DDT). Later, the strip-yield model was generalised to take into account the plate thickness using the first-order (or Kane and Mindlin) plate theory and the fundamental solution for an edge dislocation in a finite thickness plate [12]. This allowed the solution of the same problem but for a plate of finite thickness using the DDT and the Chebyshev–Gauss quadrature method [13]. This technique was subsequently used to investigate crack retardation phenomena caused by an overload [14], local plastic collapse in a plate weakened by two closely spaced collinear cracks [15], and extended to determine the constraint factor for edge cracks with an approximate solution [16].

The solution for an embedded crack in plane stress growing under constant amplitude loading in a self-similar plastic wake was addressed by Rose & Wang [17] using the strip-yield model and the DDT in conjunction with complex potential theory. Using this approach, the boundary value problem for the minimum stress state was expressed as a Riemann–Hilbert problem, and the solution derived in the form of a

* Corresponding author.
E-mail address: andrei.kotousov@adelaide.edu.au (A. Kotousov).

https://doi.org/10.1016/j.tafmec.2023.104034
Received 3 July 2023; Received in revised form 27 July 2023; Accepted 27 July 2023
Available online 9 August 2023

sum of singular integrals, requiring numerical methods to solve. However, a complete analysis of the opening and closing mechanisms was not undertaken in that study. The same approach was later extended to consider the case of plane strain, allowing the calculation of constraint factors through comparison with a finite element model [18]. The DDT has also been used to solve crack problems in piezoelectromagnetic media [19], and for problems involving frictional contact between crack faces [20].

Obtaining analytical results for more general geometries and loading conditions poses significant challenges. Therefore, since the early 1980s the application of the strip-yield model has primarily been driven by its implementation into various computational procedures and the development of software packages such as FASTRAN and NASGRO [21,22]. These packages have become very popular in the evaluation of the life of structural components subject to variable amplitude loading in the high-cycle fatigue regime. The existing computational procedures normally discretise the crack and the plastic strip ahead of the crack tip using finite elements to represent the free-from-stress, contact, direct and reverse plasticity zones. Due to computational constraints, the number of these finite elements is limited and the length is usually described by an empirical function. The accuracy and convergence of the numerical procedures have not been properly addressed in the literature, in part due to the absence of analytical solutions for finite crack geometries. Numerical predictions using software packages can be affected by the 2D nature of the underlying methodology and strip-yield assumption, the selection of the cycle counting algorithm (in the case of variable amplitude loading), discretisation, and the implementation of numerical schemes to identity crack opening and closure. The current work can help to address the latter issues.

In this paper we present a general method to analyse fatigue cracks with an arbitrary shape of the wake of plasticity. This method is based on the DDT, which is used to formulate boundary value problems describing the opening and closing process. The resulting singular integral equations feature a Cauchy kernel, and are solved using Chebyshev–Gauss quadrature. This method is applied to obtain an exact solution for an embedded fatigue crack of finite length propagating under constant amplitude cyclic loading – a problem that is commonly observed in practical applications. Exact values of the crack tip opening stress as a function of the R-ratio and the ratio of the maximum stress to the yield stress are reported for the first time. Similarly, the stress at which the crack faces first make contact, as well as the location of the contact point, is derived. The necessary modifications and considerations needed to apply the method to a wake of plasticity that does not satisfy the self-similarity condition are also briefly outlined. The obtained solution can be used to calculate the effective stress intensity factor and provide fatigue life estimates by correlation with the crack growth rates. This solution, as mentioned above, can also be used to validate the numerical procedures mentioned above, which also utilise the strip-yield methodology.

The paper is structured as follows: Section 2 provides a mathematical problem formulation including the governing equations and the appropriate boundary conditions associated with the various stages of crack closure or opening. Section 3 briefly outlines the application of the DDT to the formulated boundary-value problems. Section 4 describes a validation and convergence study using the exact solution for the maximum stress state, and comparison with small-scale yielding results for the minimum stress state. In Section 5, new results for the crack tip opening stress and the contact stress are presented and compared with past numerical studies. In particular, it is shown that crack face contact precedes closure at the tip, similar to the semi-infinite crack case considered by Budiansky and Hutchinson. It seems, that this effect is beyond the modelling capabilities of the existing numerical procedures as it has never been reported in numerical simulations. The contact stress is also derived, and plots of the crack tip stretch during a single load cycle are presented. Section 5.3 discusses the application of the method to fatigue cracks for which the shape of the plastic wake is nonlinear, and for cracks subjected to variable amplitude cyclic loading. Finally, a summary of the outcomes of this work and a brief demonstration of some the future applications of the developed method are discussed.

2. Problem formulation

Consider an infinite plate containing a through-thickness embedded crack of length $2a$, subjected to mode I cyclic loading with the stress range $\Delta\sigma = \sigma_{\max} - \sigma_{\min}$ and load ratio $R = \sigma_{\min}/\sigma_{\max}$. Plane stress conditions are assumed, and the material has Young's modulus E, and yield stress σ_Y. As discussed in the introduction, the strip-yield model [9], which is appropriate for plane stress conditions, is employed to model elastic–plastic effects. Due to the absence of any length scale other than the size of the crack itself, the wake of plasticity may be assumed to be self-similar [17,23], i.e. proportional to $|x|$.

2.1. Maximum stress

In accordance with the crack closure phenomenon, the fatigue process is associated with the formation of a wake of plasticity, represented by the addition of plastically deformed material to the faces of the crack [11], shown schematically in Fig. 1. For $\sigma_{yy} = \sigma_{\max}$, a zone of direct plastic yielding exists ahead of the crack tips, as shown in Fig. 1(a), and the corresponding boundary conditions are

$$\sigma_{yy}(x) = \begin{cases} 0, & |x| < a, \\ \sigma_Y, & a < |x| < b, \end{cases} \tag{1a}$$

$$\sigma_{yy} \to \sigma_{\max}, \quad r \to \infty. \tag{1b}$$

Combined with the equilibrium equations and the requirement that the stresses remain bounded, Eq. (1) allows for the determination of the ratio of the size of the crack to the extent of the plastic zone, a/b, and the distribution of plastic stretch, $\delta_{\max}$, in terms of $\sigma_{\max}/\sigma_Y$, where the plastic stretch is defined in terms of the displacement at the crack face, u_y, as $\delta = u_y(0^+) - u_y(0^-)$.

2.2. Minimum stress

For the minimum stress state, the extended crack consists of four distinct intervals, shown in Fig. 1(b). The residual plastic wake closes the crack in the interval $l < |x| < a$, while the central part of the crack, $|x| < l$, is assumed to remain open. Due to the self-similarity assumption, the plastic stretch in $l < |x| < a$ is proportional to $|x|$. Ahead of the crack, for $a < |x| < d$, a zone of reverse plasticity is formed, while the plastic stretch otherwise remains identical to the conditions at the maximum stress.

Based on the above considerations, the boundary conditions appropriate for $\sigma_{\min}$ are

$$\sigma_{yy}(x) = \begin{cases} 0, & |x| < l, \\ -\sigma_Y, & a < |x| < d, \end{cases} \tag{2a}$$

$$\sigma_{yy} \to \sigma_{\min}, \quad r \to \infty \tag{2b}$$

for the stress, and

$$\delta_{\min}(x) = \begin{cases} \delta_R\,|x/a|\,, & l < |x| < a, \\ \delta_{\max}(x), & d < |x| < b \end{cases} \tag{2c}$$

for the plastic stretch, in addition to the requirement that the stress be bounded. The parameters l, d and δ_R are uniquely determined by Eq. (2) as functions of $\sigma_{\max}/\sigma_Y$ and $R = \sigma_{\min}/\sigma_{\max}$ based on the solution to Eq. (1).

As discussed in Ref. [17], the solution to the present problems may be derived independently of the material properties σ_Y and E, provided that the results are presented in terms of appropriately chosen nondimensional parameters.

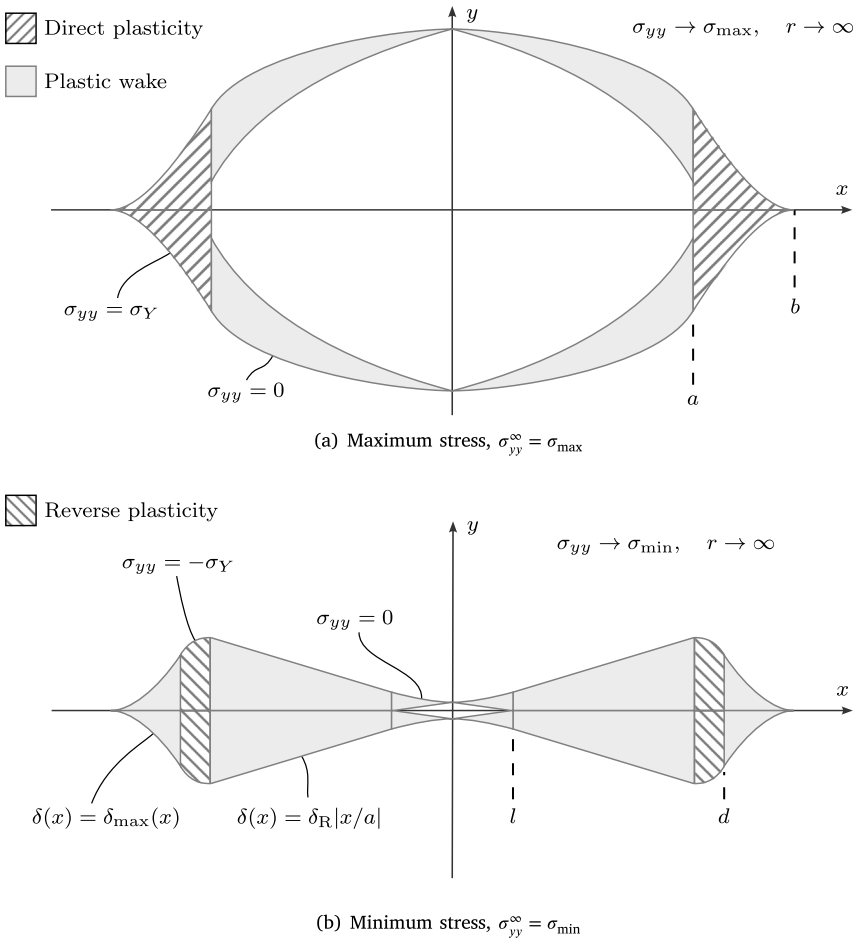

Fig. 1. Crack closure schematics based on the Dugdale model and assuming a linear plastic wake, showing (a) the maximum stress and (b) minimum stress states (the deformations are exaggerated for clarity). The intervals for the boundary conditions are shown in the right half plane, and the corresponding prescribed values of the stress or plastic stretch in the left half plane. The direct and reverse plasticity zones, as well as the plastic stretch are indicated using hatching and shading shown in the legend; the crack opening is the blank region in the middle of the crack.

2.3. Crack closure process

If the stresses and displacements at maximum and minimum stress are known, the intermediate stages of the crack opening and closing process during cyclic loading may be studied in detail. Schematic diagrams of each stage are shown in Fig. 2. This section formulates boundary value problems to determine the opening stress, the contact stress, and the variation in the crack-tip stretch during a stress cycle.

When the applied stress is $\sigma_{\min}$, the contact points are located at $x = \pm l$. As the stress increases, the contact points advance towards the crack tips through purely elastic deformation, reaching the crack tips $x = \pm a$ at the opening stress σ_{op}. Ahead of the crack, the plastic stretch is unchanged from its value at $\sigma_{\min}$. The opening stress is used in crack closure models to predict $\Delta\sigma_{\text{eff}} = \sigma_{\max} - \sigma_{\text{op}}$ and the effective stress intensity factor range, ΔK_{eff}, and as such is of critical importance in predicting crack growth rates and hence estimating the fatigue life [3]. The problem formulation may easily be adapted from the equivalent problem for a semi-infinite crack [11] (a schematic is shown in Fig. 2(c)). The boundary conditions corresponding to the opening stress state are

$$\sigma_{yy}(x) = 0, \quad |x| < a \tag{3a}$$

$$\delta_{\text{op}}(x) = \delta_{\min}(x), \quad a < |x| < b \tag{3b}$$

$$\sigma_{yy} \to \sigma_{\text{op}}, \quad r \to \infty. \tag{3c}$$

Any subsequent increase in loading above σ_{op} is accompanied by the spread of direct plastic yielding from the crack tips towards $x = \pm b$, eventually attaining the maximum stress state.

The unloading process is accompanied by the immediate removal of the direct plasticity zone and the spread of a zone of reverse plastic yielding from the crack tip, shown in Fig. 2(d). Budiansky & Hutchinson [11] showed that, for a semi-infinite crack, the surfaces of the crack first make contact at a small distance from the crack tips, and the same holds for the finite length crack considered here. The point of first contact is shown in Fig. 2(e); the stress at which contact first occurs is denoted σ_{cont}, the location of contact by l_c and the extent of the plastic zone at contact by d_c (see the schematic in Fig. 2(e)). The corresponding boundary conditions are

$$\sigma_{yy}(x) = \begin{cases} 0, & |x| < a, \\ -\sigma_Y, & a < |x| < d_c, \end{cases} \tag{4a}$$

$$\delta_{\text{cont}}(x) = \delta_{\max}(x), \quad d_c < |x| < b, \tag{4b}$$

$$\sigma_{yy} \to \sigma_{\text{cont}}, \quad r \to \infty \tag{4c}$$

combined with the requirement that d_c be the minimum value for which there exists a real root on the interval $l < x < a$ to the equation

$$\delta_{\text{cont}}(x) - \delta_R|x/a| = 0. \tag{4d}$$

Provided that such a root exists, it is l_c, the point of contact between the plastic wake attached to the faces of the crack.

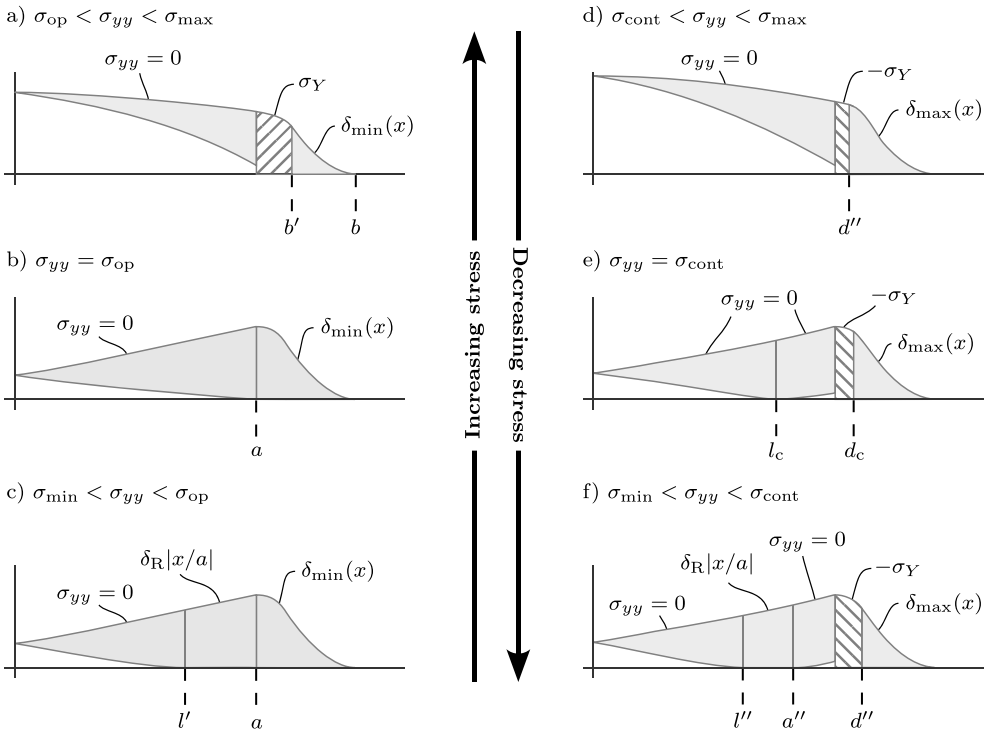

Fig. 2. Diagrams of the intermediate stages of the crack opening and closing processes between the maximum and minimum stress states shown in Fig. 1. The respective stress ranges and all boundary conditions are displayed for each stage (only half the crack is shown, for compactness). Deformations are exaggerated for clarity.

To avoid repetition, the boundary conditions for the states shown in Fig. 2(a), (c) and (d) are omitted, as they are straightforward modifications of those given above. The state shown in (f), the behaviour after unloading beyond the first contact between the faces of the crack, i.e. for $\sigma_{min} < \sigma_{yy} < \sigma_{cont}$ is more complicated. Reduction in the load below σ_{cont} leads to the initial point of contact l_c spreading in both directions, accompanied by further increase in the extent of the reverse yielding zone. Then, there are multiple contact-free zones, one at the centre of the crack ($|x| < l''$), and one at each crack tip ($a'' < |x| < a$). The boundary conditions are

$$\sigma_{yy}(x) = \begin{cases} 0, & |x| < l'' \text{ and } a'' < |x| < a \\ -\sigma_Y, & a < |x| < d_c, \end{cases} \tag{5a}$$

$$\delta_{cont}(x) = \begin{cases} \delta_R\,|x/a|\,, & l'' < |x| < a'', \\ \delta_{max}(x), & d'' < |x| < b, \end{cases} \tag{5b}$$

$$\sigma_{yy} \to \sigma_{cont}, \quad r \to \infty. \tag{5c}$$

Eventually, when the minimum stress is attained, the central zone reaches $x = \pm l$, the crack tip zones reach $x = \pm a$, and the reverse yielding zone reaches $x = \pm d$ simultaneously. Despite these additional complications, the solution is undertaken in analogous manner to the other solutions.

3. Distributed dislocation technique

The two problems formulated in Section 2 are boundary value problems in elasticity, and hence their solutions may be undertaken using many well-established approaches. One of the most popular approaches for the solution of plane crack problems is the DDT, described in detail in refs. [24,25]. Using this method, the crack is represented by a distribution of edge dislocations along the faces of the crack. The density of dislocations, B, is then related to the boundary conditions through an integral equation, for which many efficient solution strategies have been developed.

The stress distribution associated with a distribution of dislocations with density B is obtained from the solution for a single edge dislocation in plane stress using the Green's function method,

$$\sigma_{yy}(x, y) = \frac{E}{4\pi} \int_{-b}^{b} B(\xi) G_{yyy}\, d\xi \tag{6}$$

where G_{yyy} denote the stress influence function associated with a single edge dislocation located at $x = \xi$, $y = 0$. For an infinite medium the stress influence function is

$$G_{yyy} = \frac{x_1(x_1^2 + 3y^2)}{r^4} \tag{7}$$

where $x_1 = x - \xi$, $r^2 = (x - \xi)^2 + y^2$. Hence, using superposition, the normal stress along the crack line $y = 0$ in the presence of a uniform remote stress σ_{yy}^{∞} is

$$\sigma_{yy}(x, 0) = \sigma_{yy}^{\infty} + \frac{E}{4\pi} \int_{-b}^{b} \frac{B(\xi)}{x - \xi}\, d\xi. \tag{8}$$

Similarly, the crack opening/plastic stretch is

$$\delta(x) = \int_{x}^{b} B(\xi)\, d\xi. \tag{9}$$

When applied to the boundary value problems formulated in Section 2, Eq. (8) may be recognised as a singular integral equation containing a Cauchy kernel for the unknown dislocation density B. Such equations may be inverted using analytic function methods or numerical methods. In the present work, a numerical solution is derived using the Chebyshev–Gauss quadrature method: a brief background on this approach is presented in Appendix A. The approach represents B as the product of an appropriately chosen weight function and a series in the Chebyshev polynomials of the second kind,

$$B(s) = \phi(s)\sqrt{1 - s^2}, \quad \phi(s) = \sum_{j=0}^{N} \alpha_j U_j(s) \tag{10}$$

using integration points s, collocation points t and quadrature weights W given in the appendix. The Chebyshev–Gauss quadrature method

applied to Eqs. (8) and (9) provides

$$\sigma(t_k) = \sigma^{\infty}_{yy} + \frac{E}{4}\sum_{i=1}^{N}\frac{W_i\phi(s_i)}{t_k - s_i} \tag{11}$$

$$\delta(t_k) = b\pi\sum_{i=1}^{N} W_i\phi(s_i)\theta(s_i - t_k) \tag{12}$$

where θ denotes the unit step function, and $\sigma(t_k)$ and $\delta(t_k)$ are the prescribed values of the stress and crack opening/plastic stretch at the integration points. All the boundary value problems in Section 2 may be interpreted as a system of $N+1$ linear equations for the values of ϕ at the N integration points. The requirement of bounded stresses at all points provides an extra condition, and allows the solution of the system in matrix form.

Specifically, a residual for the problem may be defined in terms of the discontinuity in the dislocation density at the junction between two boundary conditions. Physically this corresponds to removing the stress singularity at each respective point. Denoting this set of points by p, the residual for a particular problem may then be defined

$$R(\phi) = \sum_p [B_p]^2 = \sum_p [B(p^+) - B(p^-)]^2 \tag{13}$$

where $B(p^+)$ and $B(p^-)$ are, respectively, the values of B just ahead of and just behind p, calculated using Eq. (10). The solution may then be derived by iteration from an initial guess for ϕ using a numerical optimisation method. If there is only one such point, then a root-finding method may be used instead for more rapid convergence. Detailed explanations of the methods used to solve these equations, and validation of the results against previous studies, are presented in Section 4, and application of those results to the analysis of the crack opening and closing process is presented in Section 5.

4. Verification

Using the Chebyshev–Gauss method, the equations for the maximum stress state are

$$\sum_{i=1}^{N}\frac{W_i\phi(s_i)}{t_k - s_i} = \begin{cases} -4\sigma_{\max}/E, & |t_k| < a/b \\ 4(\sigma_Y - \sigma_{\max})/E, & a/b < |t_k| < 1 \end{cases} \tag{14}$$

and for the minimum stress state are

$$\sum_{i=1}^{N}\frac{W_i\phi(s_i)}{t_k - s_i} = \begin{cases} -4\sigma_{\min}/E, & |t_k| < l/b \\ -4(\sigma_Y + \sigma_{\min})/E, & a/b < |t_k| < d/b \end{cases} \tag{15a}$$

$$\pi\sum_{i=1}^{N} W_i\phi(s_i)\theta(s_i - t_k) = \begin{cases} \delta_{\mathrm{R}}\,|t_k|/a, & l/b < |t_k| < a/b \\ \delta_{\max}(bt_k)/b, & d/b < |t_k| < 1. \end{cases} \tag{15b}$$

Due to the use of Chebyshev–Gauss quadrature, the length parameters on the crack (e.g. a, l and d) must be treated as a discrete rather than continuous variables, taking the locations of the quadrature points, while the applied stresses and δ_{R} are continuously varying parameters. For numerical reasons, it is most convenient to approach the problem by assigning the discrete variables and solving for the corresponding values of the continuous variables.

As an analytical solution exists for the maximum stress state, this condition is used to ensure the accuracy of the method and establish the required number of integration points, N, to achieve highly accurate results. For later reference, the analytical solution for the Dugdale model is

$$\frac{a}{b} = \cos\left(\frac{\pi\sigma_{\max}}{2\sigma_Y}\right), \quad \delta_{\mathrm{M}} = \frac{8\sigma_Y a}{\pi E}\overline{\delta_{\mathrm{M}}} = \frac{8\sigma_Y a}{\pi E}\log\frac{b}{a}. \tag{16}$$

For a given value of a, an initial guess for the maximum stress, $\sigma^{(0)}_{\max}$, allows the system Eq. (14) to be solved in the least squares sense to identify an approximate solution for the regular part of the dislocation density, ϕ_0. Then, this solution may be used to calculate a value of the residual using $R_{\max}(\phi) = [B_a]$. The solutions $\sigma_{\max}$ and ϕ may be found via iteration using a root-finding method subject to the bound $\sigma_{\max} < \sigma_Y$.

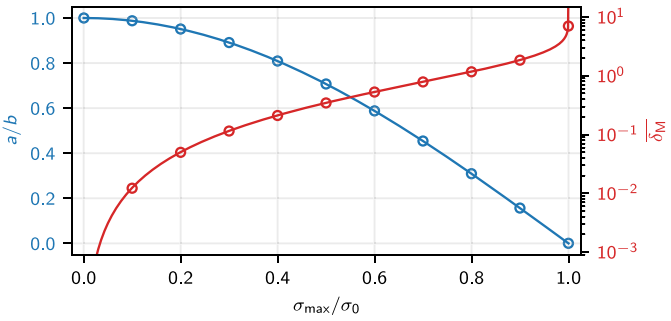

Fig. 3. Comparison between the present results for $N = 5000$ (circles) and corresponding analytical results (solid lines) for the ratio a/b (blue, left y-scale) and the normalised plastic stretch at the crack tip (red, right y-scale) in the maximum stress state for different values of $\sigma_{\max}/\sigma_Y$.

Table 1
Convergence of the maximum stress model for the nearest available value to $\sigma_{\max}/\sigma_Y = 0.5$. The estimate of the parameter $\overline{\delta_{\mathrm{M}}}$ found using the distributed dislocation technique is compared to the corresponding analytical result (the results for a/b are identical up to twelve decimal places for all tabulated values of N).

N	$\sigma_{\max}/\sigma_Y$	a/b	Method	$\overline{\delta_{\mathrm{M}}}$
25	0.461538	0.748511	DDT	0.289726731
			Exact	0.289669716
50	0.509804	0.696134	DDT	0.362228432
			Exact	0.362213186
100	0.495050	0.712584	DDT	0.338861421
			Exact	0.338857529
250	0.501992	0.704891	DDT	0.349713109
			Exact	0.349712478
500	0.499002	0.708214	DDT	0.345008542
			Exact	0.345008384
1000	0.499500	0.707661	DDT	0.345789632
			Exact	0.345789592
2000	0.499750	0.707384	DDT	0.346181251
			Exact	0.346181241
5000	0.499900	0.707218	DDT	0.346416568
			Exact	0.346416567

The results were compared to the analytical solution in Table 1 showing the rapid convergence of the quadrature method, even for low values of N; the results match to 8 decimal places for $N = 5000$. The accuracy of the results for values of $\sigma_{\max}/\sigma_Y$ not shown in the table is demonstrated in Fig. 3, showing the results for a/b and $\overline{\delta_{\mathrm{M}}}$ for $N = 5000$. It may be observed that the results are accurate across the full range of admissible values.

The minimum stress state is specified by four independent parameters: the minimum stress $\sigma_{\min}$, the contact-free length l, the maximum extent of the reverse yielding zone d and the residual plastic stretch at the crack tip δ_{R}.

The residual for the minimum stress state is

$$R_{\min}(\phi) = [B_l]^2 + [B_a]^2 + [B_d]^2 \tag{17a}$$

subject to the bounds on each parameter

$$0 < l < a, \quad a < d < b, \quad 0 < \delta_{\mathrm{R}} < \delta_{\mathrm{M}}, \quad \sigma_{\min} < \sigma_{\max}. \tag{17b}$$

The solution is identified through the minimisation of Eq. (17a) via a multidimensional optimisation algorithm. Due to the use of Chebyshev–Gauss quadrature, l and d can only be placed at integration points, and therefore accurate values are obtained by interpolation where necessary. The value of N chosen for the analysis affects the resolution of the mesh at the crack. For low values of N the Chebyshev–Gauss quadrature points are coarsely spaced close to the centre of the crack, which has implications on the values of the contact-free length parameter, l, that can be obtained from the solution. As the present

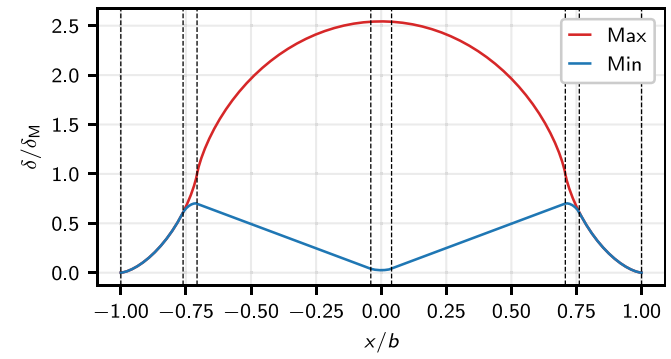

(a) Crack opening/plastic stretch

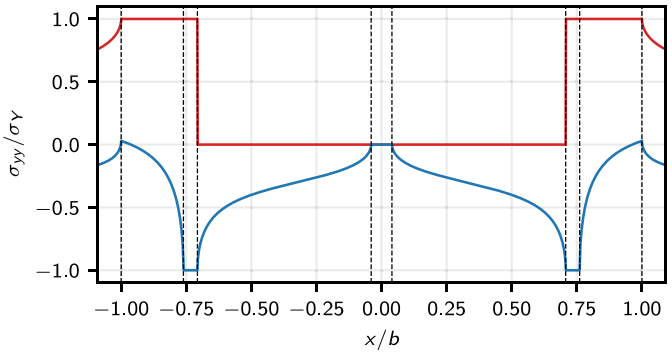

(b) Stress normal to the crack

Fig. 4. Plots for the maximum stress (red) and minimum stress (blue) states of (a) the crack opening/plastic stretch, and (b) the normal stress at the crack surfaces. The dashed black lines show the intervals in Fig. 1. The data is plotted for the values given in Eq. (18).

work is focused on providing accurate results over the widest possible parameter ranges, $N = 5000$ was selected. Having established accurate values using $N = 5000$, future studies may be based on lower values of N, which would be more feasible for practical calculation.

Example plots of the dislocation density, crack opening/plastic stretch, and stress distribution at the minimum stress state for

$$N = 5000, \quad \sigma_{max}/\sigma_Y = 0.4999, \quad a/b = 0.707\,22,$$
$$\mathrm{R} = -0.531\,39, \quad \delta_R/\delta_M = 0.700\,05, \quad l/b = 0.039\,88, \quad d/b = 0.760\,91 \tag{18}$$

are presented in Fig. 4, indicating the locations $x = \pm l, \pm a, \pm d$, showing the shape of the plastic wake, and demonstrating that the boundary conditions in Eq. (2) are satisfied. An excerpt of the numerical results for several different values of σ_{max}/σ_Y and R are provided in Appendix B. Though Rose & Wang [17] derived an analytical solution for the minimum stress state, a full comparison with the results of this study is not possible, as those results were only presented in graphical form. However, based on a comparison of the trends and observation of some specific values, those results appear in excellent agreement with the present results. Budiansky & Hutchinson reported the numerical values $\delta_R/\delta_M = 0.8562$ and $(d-a)/(b-a) = 0.092\,86$ for $\mathrm{R} = 0$ assuming small-scale yielding (i.e. in the limit $\sigma_{max}/\sigma_Y \to 0$). For $\sigma_{max}/\sigma_Y = 0.1$ and $\mathrm{R} = 0$, the present results provide 0.849 81 and 0.097 798 respectively, which suggests that the small-scale yielding results are recovered as $\sigma_{max}/\sigma_Y \to 0$.

5. Crack opening and closing process

After determination of the maximum and minimum stress states, the opening and closing process may be studied using the boundary conditions formulated in Section 2.3.

5.1. Opening and contact stresses

Eq. (3) depends on both the minimum and maximum stress states through a and δ_{min}, but otherwise contains only one unknown parameter, σ_{op}, and may be solved using the same Chebyshev–Gauss method described above, by iterating through values of σ_{op} to remove the singularity at the crack tips $x = \pm a$, with the restriction $\sigma_{min} < \sigma_{op} < \sigma_{max}$.

Plots of the solution for the opening stress normalised to the maximum stress for different R-ratios and σ_{max}/σ_Y are presented in Fig. 5, showing that the crack opens earlier for lower values of R, and the curves coalesce as $\mathrm{R} \to 1$. Fig. 5 also shows the results for the opening stress presented by Newman [26], based on empirical equations fit to numerical results for a centre crack tension specimen of arbitrary plate thickness. The present results display a generally similar trend to those of Newman for both R and σ_{max}/σ_Y, though there is a significant discrepancy between the predicted values, especially close to $\mathrm{R} = -1$, and for high values of σ_{max}/σ_Y. Though an experimental study was not undertaken in the present work, a limited comparison may be made through Newman's results, which have been used in experimental studies to determine fatigue crack growth rates. One such study [3] found that Newman's model was highly accurate for several values of R. However, the comparison in that work was limited to $\sigma_{max}/\sigma_Y = 0.33$, for which the present results and Newman's results are very similar (see Fig. 5). A more complete investigation of the accuracy of the present results should focus on higher values of σ_{max}/σ_Y, at which the discrepancies are more pronounced.

The contact stress may be derived by applying the same method described in Section 3 to Eq. (4), though now the additional condition Eq. (4d) must be checked for each potential solution to ensure that no interpenetration of the crack faces occurs. The correct solution, at which contact first occurs, may be rapidly identified using a bisection method. Plots of the contact stress normalised to the maximum stress are presented in Fig. 6, also showing the normalised opening stress for the same conditions.

The present results for $\sigma_{max}/\sigma_Y = 0.1$, $\mathrm{R} = 0$ provide $\sigma_{op}/\sigma_{max} = 0.537\,43$ and $\sigma_{cont}/\sigma_{max} = 0.469\,54$. Based on the tendencies shown in Fig. 6, it is likely that in the small-scale yielding limit Budiansky & Hutchinson's results of $K_{op}/K_{max} = 0.557$ and $K_{cont}/K_{max} = 0.483$ are recovered. Numerical values of σ_{op}/σ_{max}, $\sigma_{cont}/\sigma_{max}$, l_c/a and d_c/a are presented the table in Appendix B. Note that the contact point is typically extremely close to the crack tip for low values of σ_{max}/σ_Y, though it is generally further away for low and negative values of R.

5.2. Cyclic crack tip stretch

Based on parameters derived above, the full details of each state of the crack opening and closing processes may be derived. In this section, we focus on the per cycle variation in the plastic stretch at the crack tips $x = \pm a$ during a single cycle. This part of the solution is among the most laborious, as it requires analysis of several different problems depending on the value of the applied stress, shown in Fig. 2(a), (c), (d), (f). The part of the stress cycle with $\sigma_{min} < \sigma_{yy} < \sigma_{cont}$ is the most problematic, as it requires iteration to determine the parameters l'', a'' and d'' matching a given value of the applied stress. This part of the solution was omitted by Budiansky & Hutchinson; however, it is analysed in full here to identify the closure process at the crack tip.

Selected results for $\sigma_{max}/\sigma_Y = 0.5$ are shown in Fig. 7 for $\mathrm{R} = -1$, 0 and 0.4 with the maximum stress, minimum stress, opening stress, and contact stress indicated. As expected, between σ_{min} and σ_{op}, when the response is purely elastic, there is no change in the plastic stretch. Subsequently it increases smoothly to a maximum of δ_M at σ_{max}, and then decreases smoothly until σ_{min}. The unloading stage is identical for all values of R until σ_{cont}, as the boundary conditions for this part of the cycle only depend on the data at the maximum stress. The final stage of unloading, for stresses below σ_{cont}, is characterised by a smooth

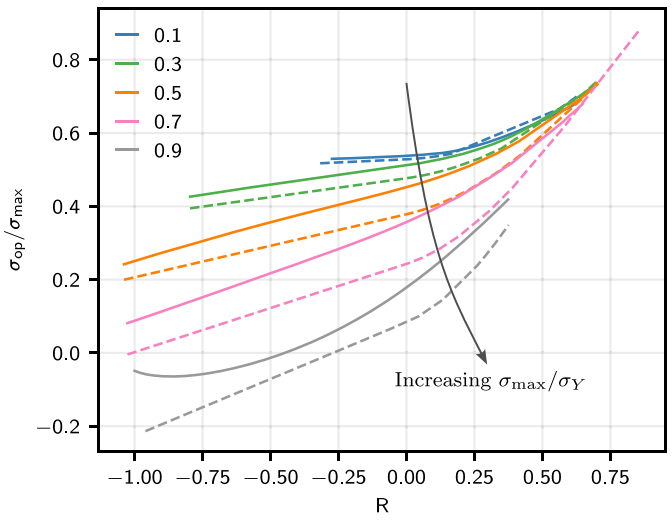

(a) Variation with R for fixed σ_{max}/σ_Y

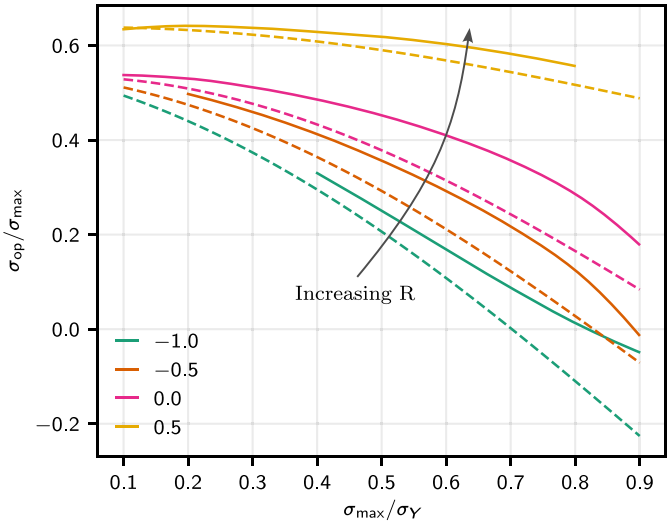

(b) Variation with σ_{max}/σ_Y for fixed R

Fig. 5. Opening stress normalised to the maximum stress plotted for (a) R and (b) σ_{max}/σ_Y. The present results are shown with solid lines, the dashed lines show the predictions from Ref. [26] for plane stress.

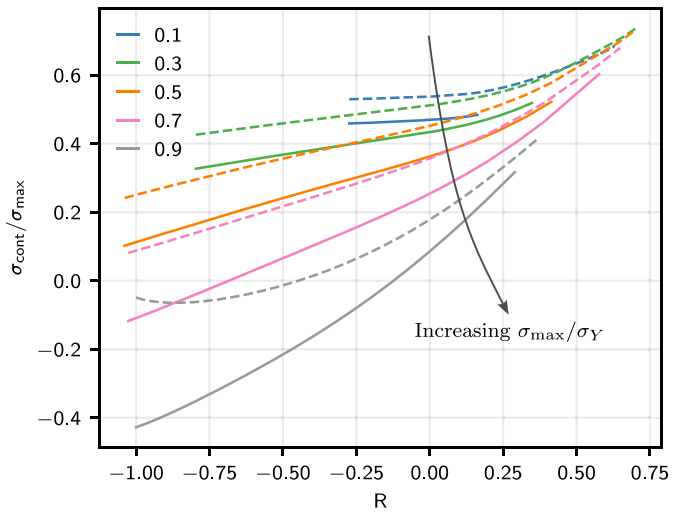

(a) Variation with R for fixed σ_{max}/σ_Y

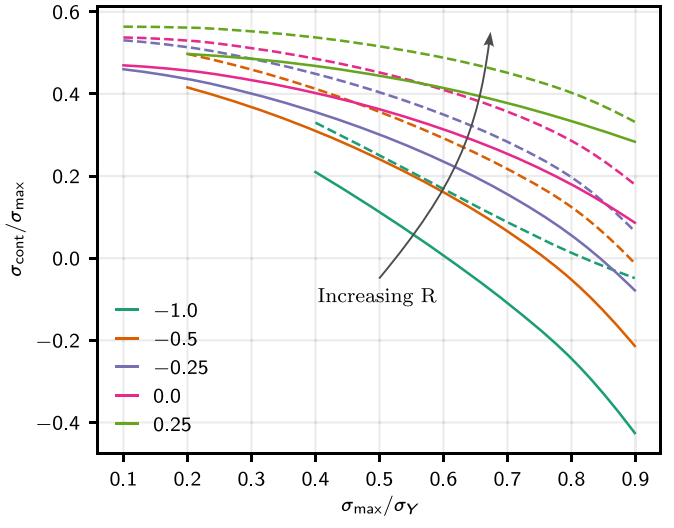

(b) Variation with σ_{max}/σ_Y for fixed R

Fig. 6. Contact stress normalised to the maximum stress plotted for (a) R and (b) σ_{max}/σ_Y. The contact stress is shown with solid lines, the dashed lines show the corresponding opening stress.

reduction in the crack tip stretch, attaining the minimum stress value, δ_R, at σ_{min}. It can also be observed that the stages before opening and after contact occupy proportionally more of the cycle for low and negative values of R.

5.3. Power law plastic wake

The results presented above were derived for a linear plastic wake, appropriate for the assumption of constant amplitude cyclic loading: for variable amplitude cyclic loading, on the other hand, it is not possible to identify the specific form of the wake without recourse to experimental data. However, if a reasonable shape of the plastic wake were identified, the present method would allow the solution to be easily calculated. For example, the simplest generalisation would be a wake following a power law of degree n; the case $n = 1/2$, corresponding to a square-root shape is considered here. The maximum stress state is unchanged, and the boundary conditions for the minimum stress state are almost identical, with the exception of the plastic stretch in the closed portion of the crack, which is replaced by $\delta_{min}(x) = \delta_R\sqrt{|x/a_0|}$, where a_0 is an additional length scale for the problem. Hence, the problem variables must be regarded as functions of R, σ_{max}/σ_Y, and a/a_0.

The solution procedure described above then allows the calculation of the parameters l/a, d/a, δ_R and σ_{min} with no other changes. An example plot of the crack opening/plastic stretch and stress distribution at the crack faces for $\sigma_{max}/\sigma_Y = 0.5$, R $= -0.0404$ and $a_0 = a$ is shown in Fig. 8. Though the computational time for the solution increases considerably compared to the self-similar case due to the introduction of an extra parameter, the present approach remains valid.

6. Conclusion

This paper describes a method for the analysis of the closure of propagating cracks due to the presence of a wake of plasticity. New analytical results are obtained for an embedded crack propagating under constant amplitude cyclic loading. The present results are consistent, in terms of the general trends, with past numerical simulations

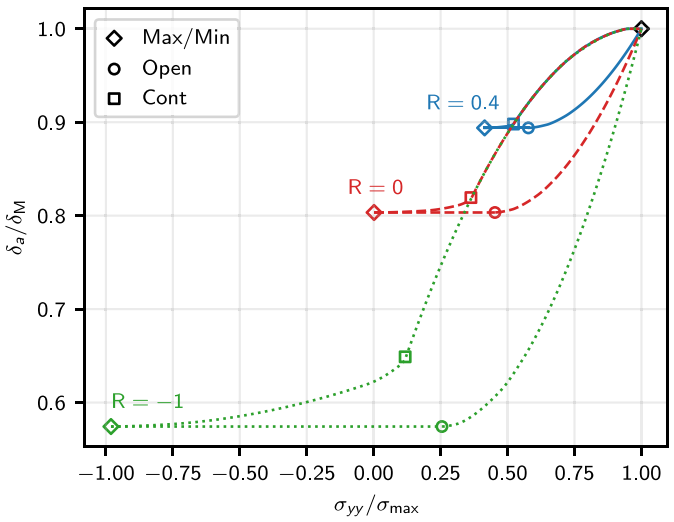

Fig. 7. Cyclic plastic stretch at the crack tip for $\sigma_{max}/\sigma_Y = 0.5$ for three values of R. The opening stress, contact stress and maximum and minimum stresses for each case are marked.

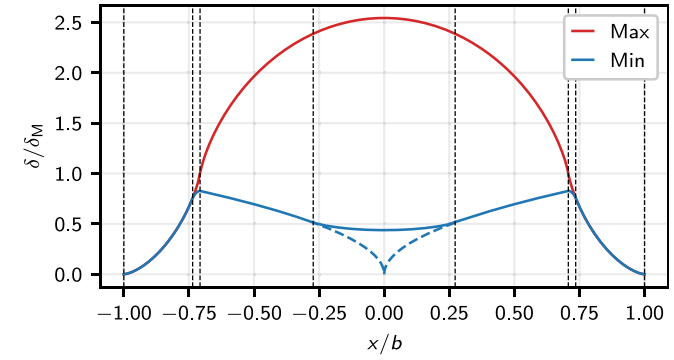

(a) Crack opening/plastic stretch

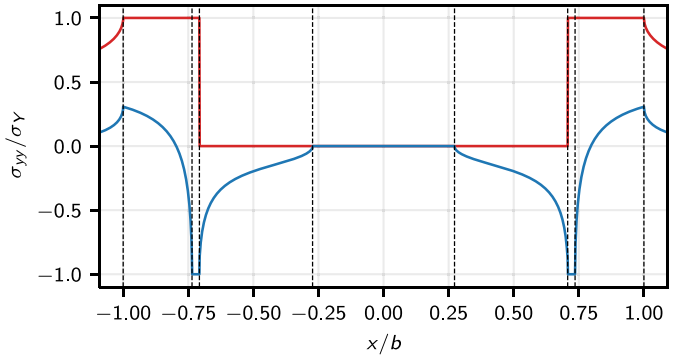

(b) Stress normal to the crack

Fig. 8. Example plots, for a power law plastic wake, of the maximum stress (red) and minimum stress (blue) states of (a) the crack opening/plastic stretch, and (b) the normal stress at the crack surfaces. The dashed black lines show the intervals in Eq. (2), and the dashed line in (a) shows the shape of the plastic wake over the contact-free length. The data is plotted for $\sigma_{max}/\sigma_Y = 0.5$ and R = −0.0404.

utilising the same methodology and the plane stress assumption. The results also recover analytical results in the small-scale yielding limit. The finding that the first contact during unloading does not occur at the crack tips, in agreement with Budiansky & Hutchinson's result for a semi-infinite crack, has to the best knowledge of the authors, not been incorporated into numerical procedures or reported in published outcomes of numerical simulations. It was also conclusively shown that closure at the crack tip is not achieved until the minimum stress, via solution of the post-contact response of the crack, an analysis that was omitted from previous small-scale yielding analyses. Finally, the extension of the present results to more general shapes of the plastic wake was outlined and demonstrated using a simple example.

One advantage of the method developed in this work is that it is straightforward to consider generalisations for other geometries or loading states by changing the boundary conditions or the integral kernel in Eq. (6). Unlike the methods employed in other analytical studies, the present work is applicable to edge cracks, which are a key contributor to the development of fatigue damage, particularly in the high-cycle regime. The present work may be adapted to consider edge cracks by modification of the kernel in the singular integral, and the points employed in the Chebyshev–Gauss quadrature. Similarly, the method could be extended beyond plane stress conditions to consider the influence of plate thickness if the first-order plate theory were employed [12], though the assumption of a linear plastic wake in this case may only be approximately satisfied. A more general shape of the plastic wake would also be necessary for other crack geometries, such as a plane crack emanating from a stress concentration (e.g. a cylindrical hole).

A comparison of the present solution for the opening stress with numerical results available in the literature demonstrates the same trends but some differences in the crack tip opening stress, particularly at low R-ratios. These differences may reflect differing assumptions, or limitations in existing numerical procedures. The obtained solution could also provide computational methods with a guide for the discretisation process, assisting in appropriately selecting the sizes of finite elements for each of the characteristic crack regions. The results for the stress values corresponding to crack face contact have not been reported in numerical simulations. Therefore, in order to understand the limitations of the existing numerical procedures, it would be necessary to investigate the importance of this effect in future studies.

Funding

This research was partially supported by the Australian Government through the Australian Research Council's Discovery Projects funding scheme (project DP200102300).

Declaration of competing interest

The authors declare that they have no known competing financial interests or personal relationships that could have appeared to influence the work reported in this paper.

Data availability

Data will be made available on request.

Appendix A. Chebyshev–Gauss quadrature

Substituting $x = bt$ and $\xi = bs$ into Eq. (8),

$$\sigma_{yy}(x,0) = \sigma_{yy}^{\infty} + \frac{E}{4\pi}\int_{-1}^{1}\frac{B(s)}{t-s}\,ds. \tag{A.1}$$

The integral equation may be efficiently inverted by decomposing the dislocation density into the product of a regular function, ϕ, and a weight function with appropriate asymptotic behaviour, ω, i.e.

$$B(s) = \omega(s)\phi(s). \tag{A.2}$$

Table B.2
Selected numerical results for several values of σ_{max}/σ_Y, showing the parameters associated with the maximum stress, minimum stress, opening stress and contact stress states (see Section 2 for definitions of each parameter).

σ_{max}/σ_Y	a/b	$\overline{\delta_M}$	R	l/a	d/a	δ_R/δ_M	σ_{op}/σ_{max}	$\sigma_{cont}/\sigma_{max}$	l_c/a	d_c/a
0.1	0.98769	0.01238	−0.24224	0.00223	1.00127	0.84396	0.53071	0.460257	0.99965	1.00108
			−0.11041	0.05562	1.00124	0.84709	0.53431	0.465168	0.99965	1.00106
			0.003242	0.58025	1.00122	0.84981	0.53733	0.46954	0.99965	1.00105
			0.163263	0.97333	1.00113	0.85895	0.54906	0.484216	0.99974	1.001
0.3	0.89105	0.11536	−0.73553	0.00176	1.01952	0.76083	0.4333	0.33565	0.99204	1.01311
			−0.24654	0.10875	1.01469	0.811	0.48611	0.40139	0.99532	1.01075
			0.000743	0.57935	1.01268	0.83287	0.51174	0.433812	0.99662	1.00968
			0.183543	0.89373	1.0108	0.85393	0.53828	0.467724	0.99727	1.00862
			0.349399	0.97209	1.00837	0.88275	0.57896	0.519431	0.99824	1.00713
0.5	0.70722	0.34642	−0.98114	0.00222	1.11983	0.57434	0.255	0.117551	0.92624	1.06477
			−0.53139	0.05728	1.0762	0.70005	0.35032	0.233372	0.96909	1.04865
			0.001538	0.63111	1.04511	0.80339	0.45273	0.363175	0.98832	1.03362
			0.229591	0.89258	1.03286	0.84919	0.50965	0.436198	0.99334	1.0265
			0.41432	0.9707	1.02191	0.89391	0.57769	0.522169	0.99716	1.01929
0.7	0.45419	0.78925	−0.99210	0.00346	1.49762	0.36902	0.08975	−0.10644	0.71303	1.22177
			−0.50641	0.16375	1.2442	0.60501	0.21569	0.063507	0.91721	1.15213
			0.00714	0.7346	1.11968	0.76969	0.35932	0.257226	0.97714	1.09269
			0.302103	0.94166	1.06638	0.85931	0.47601	0.408751	0.992	1.05822

In the problems under consideration the stresses are bounded at both ends, and hence $\omega(s) = \sqrt{1-s^2}$. Accordingly, ϕ is expanded as a series in the Chebyshev polynomials of the second kind,

$$\phi(s) = \sum_{j=0}^{N} \alpha_j U_j(s) \tag{A.3}$$

where N is the number of discrete integration points to be used in the quadrature scheme. For the purposes of the DDT, the integration points s_i and collocation points t_k are the roots of the Chebyshev polynomials U_N and T_{N+1} respectively,

$$s_i = \cos\frac{\pi i}{N+1}, \quad i = 1, \dots, N \tag{A.4}$$

$$t_k = \cos\frac{\pi(2k-1)}{2(N+1)}, \quad k = 1, \dots, N+1 \tag{A.5}$$

and the quadrature weights are

$$W_i = \frac{1-s_i^2}{N+1}. \tag{A.6}$$

Using Eq. (A.1) and the identities

$$\int_{-1}^{1} \frac{\sqrt{1-s^2}}{t-s} U_j(s)\, ds = \pi T_{j+1}(t) \tag{A.7}$$

$$\sum_{i=1}^{N} \frac{W_i}{t_k - s_i} U_j(s_i) = T_{j+1}(t_k), \tag{A.8}$$

the normal traction on the faces of the crack at the collocation points, $\sigma(t_k)$ is related to the values of ϕ at the integration points via

$$\sigma(t_k) = \sigma_{yy}^{\infty} + \frac{E}{4} \sum_{i=1}^{N} \frac{W_i \phi(s_i)}{t_k - s_i}, \quad k = 1, \dots, N+1. \tag{A.9}$$

Similarly, δ is calculated using an equivalent form of Eq. (9),

$$\delta = \int_{-b}^{b} B(\xi)\theta(\xi - x)\, d\xi, \tag{A.10}$$

where θ is the unit step function

$$\theta(t) = \begin{cases} 0, & t < 0 \\ 1, & t \geq 0. \end{cases} \tag{A.11}$$

Then, the Chebyshev–Gauss quadrature formula for regular integrals,

$$\int_{-1}^{1} f(s)\sqrt{1-s^2}\, ds \approx \sum_{i=1}^{N} W_i f(s_i), \tag{A.12}$$

provides

$$\delta(t_k) = b\pi \sum_{i=1}^{N} W_i \phi(s_i)\theta(s_i - t_k). \tag{A.13}$$

Using Eqs. (A.9) and (A.13) in combination with Eqs. (1) and (2) leads to Eqs. (14) and (15) of the main text, the governing equations of the maximum and minimum stress states appropriate for numerical evaluation.

Appendix B. Tabulated numerical results

Selected numerical results for the minimum stress state and crack opening and closing process are tabulated in Table B.2.

References

[1] W. Elber, Fatigue crack closure under cyclic tension, Eng. Fract. Mech. 2 (1) (1970) 37–45, http://dx.doi.org/10.1016/0013-7944(70)90028-7.

[2] J. Newman, K. Walker, Fatigue-crack growth in two aluminum alloys and crack-closure analyses under constant-amplitude and spectrum loading, Theor. Appl. Fract. Mech. 100 (November 2018) (2019) 307–318, http://dx.doi.org/10.1016/j.tafmec.2019.01.029.

[3] V. Ribeiro, J. Correia, G. Lesiuk, A. Gonçalves, A. De Jesus, F. Berto, Application and discussion of various crack closure models to predict fatigue crack growth in 6061-T651 aluminium alloy, Int. J. Fatigue 153 (March) (2021) 106472, http://dx.doi.org/10.1016/j.ijfatigue.2021.106472.

[4] T. Machniewicz, Fatigue crack growth prediction models for metallic materials: Part I: Overview of prediction concepts, Fatigue Fract. Eng. Mater. Struct. 36 (4) (2013) 293–307, http://dx.doi.org/10.1111/j.1460-2695.2012.01721.x.

[5] T. Machniewicz, Fatigue crack growth prediction models for metallic materials Part II: Strip yield model - Choices and decisions, Fatigue Fract. Eng. Mater. Struct. 36 (4) (2013) 361–373, http://dx.doi.org/10.1111/ffe.12009.

[6] R. Maia, R. Branco, F.V. Antunes, M.C. Oliveira, A. Kotousov, Three-dimensional computational analysis of stress state transition in through-cracked plates, Math. Comput. Sci. 10 (3) (2016) 343–352, http://dx.doi.org/10.1007/s11786-016-0267-z.

[7] D. Camas, J. Garcia-Manrique, F. Antunes, A. Gonzalez-Herrera, Three-dimensional fatigue crack closure numerical modelling: Crack growth scheme, Theor. Appl. Fract. Mech. 108 (April) (2020) 102623, http://dx.doi.org/10.1016/j.tafmec.2020.102623.

[8] M.F. Borges, F.V. Antunes, P.A. Prates, R. Branco, A.S. Cruces, P. Lopez-Crespo, Effect of kinematic hardening parameters on fatigue crack growth, Theor. Appl. Fract. Mech. 106 (January) (2020) 102501, http://dx.doi.org/10.1016/j.tafmec.2020.102501.

[9] D. Dugdale, Yielding of steel sheets containing slits, J. Mech. Phys. Solids 8 (2) (1960) 100–104, http://dx.doi.org/10.1016/0022-5096(60)90013-2.

[10] B.A. Bilby, A.H. Cottrell, K.H. Swinden, The spread of plastic yield from a notch, Proc. R. Soc. London. Ser. A. Math. Phys. Sci. 272 (1350) (1963) 304–314, http://dx.doi.org/10.1098/rspa.1963.0055.

[11] B. Budiansky, J.W. Hutchinson, Analysis of closure in fatigue crack growth, J. Appl. Mech. 45 (2) (1978) 267–276, http://dx.doi.org/10.1115/1.3424286.

[12] A. Kotousov, C. Hui Wang, Fundamental solutions for the generalised plane strain theory, Internat. J. Engrg. Sci. 40 (15) (2002) 1775–1790, http://dx.doi.org/10.1016/S0020-7225(02)00041-1.

[13] J. Codrington, A. Kotousov, A crack closure model of fatigue crack growth in plates of finite thickness under small-scale yielding conditions, Mech. Mater. 41 (2) (2009) 165–173, http://dx.doi.org/10.1016/j.mechmat.2008.10.002.

[14] J. Codrington, A. Kotousov, Crack growth retardation following the application of an overload cycle using a strip-yield model, Eng. Fract. Mech. 76 (11) (2009) 1667–1682, http://dx.doi.org/10.1016/j.engfracmech.2009.02.021.

[15] D. Chang, A. Kotousov, A strip yield model for two collinear cracks in plates of arbitrary thickness, Int. J. Fract. 176 (1) (2012) 39–47, http://dx.doi.org/10.1007/s10704-012-9724-0.

[16] A. Khanna, A. Kotousov, M. Mohabuth, S. Bun, Three-dimensional analysis of an edge crack in a plate of finite thickness with the first-order plate theory, Theor. Appl. Fract. Mech. 95 (January) (2018) 155–163, http://dx.doi.org/10.1016/j.tafmec.2018.02.017.

[17] L.R.F. Rose, C.H. Wang, Self-similar analysis of plasticity-induced closure of small fatigue cracks, J. Mech. Phys. Solids 49 (2) (2001) 401–429, http://dx.doi.org/10.1016/S0022-5096(00)00024-7.

[18] C.H. Wang, L.R. Rose, J.C. Newman, Closure of plane-strain cracks under large-scale yielding conditions, Fatigue Fract. Eng. Mater. Struct. 25 (2) (2002) 127–139, http://dx.doi.org/10.1046/j.8756-758x.2002.00483.x.

[19] A. Vahdati, M. Salehi, M. Vahabi, J. Jafari Fesharaki, A. Ghassemi, Fracture analysis of piezoelectromagnetic medium with axisymmetric cracks, Theor. Appl. Fract. Mech. 104 (August) (2019) 102337, http://dx.doi.org/10.1016/j.tafmec.2019.102337.

[20] A. Spagnoli, A. Carpinteri, M. Terzano, Mode II crack shielding in a compressed rough crack with friction, Theor. Appl. Fract. Mech. 107 (February) (2020) 102515, http://dx.doi.org/10.1016/j.tafmec.2020.102515.

[21] J.C. Newman, Fatigue-life prediction methodology using a crack-closure model, J. Eng. Mater. Technol. 117 (4) (1995) 433–439, http://dx.doi.org/10.1115/1.2804736.

[22] A.U. de Koning, H.J. ten Hoeve, T.K. Henriksen, Description of crack growth using the strip-yield model for computation of crack opening loads, crack tip stretch, and strain rates, in: ASTM STP 1343, American Society for Testing and Materials, 1999.

[23] H. Führing, T. Seeger, Dugdale crack closure analysis of fatigue cracks under constant amplitude loading, Eng. Fract. Mech. 11 (1) (1979) 99–122, http://dx.doi.org/10.1016/0013-7944(79)90033-X.

[24] B.A. Bilby, J.D. Eshelby, Dislocations and the theory of fracture, in: H. Liebowitz (Ed.), Fracture: An Advanced Treatise, Vol. 1, Academic Press, 1968, pp. 99–182.

[25] D.A. Hills, P.A. Kelly, D.N. Dai, A.M. Korsunsky, Solution of Crack Problems, in: Solid Mechanics and Its Applications, vol. 44, Springer Netherlands, Dordrecht, 1996, http://dx.doi.org/10.1007/978-94-015-8648-1.

[26] J.C. Newman, A crack opening stress equation for fatigue crack growth, Int. J. Fract. 24 (4) (1984) R131–R135, http://dx.doi.org/10.1007/BF00020751.